Inorganic Chemistry

ARTICLE

pubs.acs.org/IC

Structural and Spectroscopic Properties of LaOF:Eu^{3+} Nanocrystals Prepared by the Sol−Gel Pechini Method

Tomasz Grzyb and Stefan Lis*

Faculty of Chemistry, Department of Rare Earths, Adam Mickiewicz University, Grunwaldzka 6, 60-780 Poznan, Poland

ABSTRACT: A new method was used to obtain Eu^{3+}-doped LaOF nanocrystals. The obtained nanocrystals were synthesized for the first time using a modified Pechini sol−gel method. The products were analyzed by X-ray powder diffraction and the Rietveld method. Optimal conditions for the synthesis were found. Luminescent properties of the tetragonal and rhombohedral LaOF:Eu^{3+} nanocrystals were investigated by collecting excitation and luminescence spectra. The most effective dopant concentrations in both hosts were found. Luminescent lifetimes were also measured. The time-resolved luminescent traces showed both a growth and a decay, which pointed to energy transfer processes between Eu^{3+} ions in the LaOF host. In order to explain these phenomena, an adequate mechanism has been proposed. Intensity parameters Ω_2, Ω_4 and quantum efficiencies were calculated using the Judd−Ofelt theory, allowing for an extensive study of the luminescent properties of Eu^{3+} ion in the LaOF matrix.

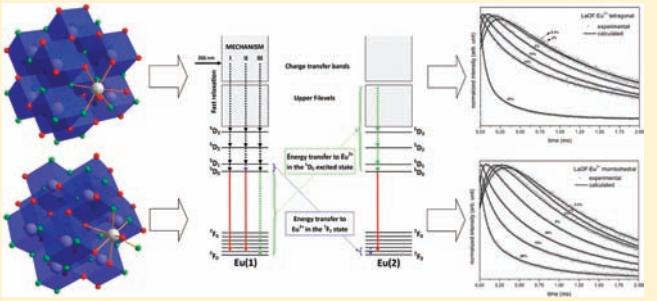

INTRODUCTION

Luminescent nanomaterials based on lanthanide-doped oxyfluorides have been intensively investigated in recent years due to their interesting properties.[1] Most of this interest is the result of the unique luminescent properties of these materials.[2] Recently, many new properties of known materials were discovered as the result of reducing the size of the crystallites.[3−5] Inorganic, lanthanide-doped materials are widely used in many applications including light-emitting devices or more complex systems like hybrid materials or biolabels.[6−10] Luminescent properties of those materials primarily follow from the physical properties of the doped lanthanide ions, but characteristics of the host compound are also important.

Lanthanide oxyfluorides doped with various Ln^{3+} ions are known from their excellent luminescent properties as UV-excited and upconversion phosphors.[11−13] Lanthanum oxyfluoride, activated by an appropriate dopant, may also be interesting for laser applications.[14] Emission in these materials results from transitions within the 4f shell of the doped ions. Properties of the host are also important factors, having influence on the luminescence of the activator ions. In REOF (rare earth oxyfluorides) crystals, quenching by the multiphonon relaxation of the excited Ln^{3+} ions is minimal. Lanthanum oxyfluoride, LaOF, is known for the low energy of its lattice phonons, whose energy is not more than 550 cm^{-1}.[15] Since the La^{3+} ion has the largest ionic radius among the lanthanide series of ions, it can be easy substituted by different Ln^{3+} ions in the structure. LaOF has also a high thermal and chemical stability.[14] Therefore, LaOF is an excellent host for the Eu^{3+} ions,[16] and as nanophosphors, they are promising candidates for practical applications.

Synthesis methods, used for the preparation of the REOF materials, are mainly based on annealing of REF_3 in air atmosphere or on solid state reactions between RE_2O_3 and REF_3 (or NH_4F).[17−19] Prepared by these methods, materials were bulk with large crystallites. To prepare a nano-REOF, different methods have to be used. The first synthesis of the nanocrystalline LaOF was reported by Lee et al. in 2003.[20] Recently, new synthesis methods have been reported, based on the decomposition of trifluoroacetates in high boiling liquids or by annealing fluorides prepared by hydrothermal methods.[12,21,22]

In this article we report the results of the synthesis of LaOF:Eu^{3+} for the first time obtained by a modified sol−gel Pechini method.[23] In this well-known method, solutions containing citric acid and ethylene glycol were used to obtain metal complexes. Heating of that mixture results in the formation of gel from the polyester.

EXPERIMENTAL SECTION

LaOF:Eu^{3+} (where the concentration of Eu^{3+} was 0.5−20% mol) nanocrystals were synthesized by the modified Pechini method. The starting materials were lanthanide oxides La_2O_3 and Eu_2O_3 (Stanford Materials 99.99%), nitric acid HNO_3 (POCh S.A., ultrapure), ammonium fluoride NH_4F (POCh S.A., ACS grade 98+%), citric acid monohydrate (CHEMPUR, p.a. grade), and ethylene glycol (CHEMPUR, p.a. grade). Lanthanide oxides were dissolved in HNO_3 and evaporated several times in order to remove an excess amount of HNO_3. To the stoichiometric amounts of the lanthanide salts dissolved in 100 mL of water, citric acid and ethylene glycol were added. A large excess of citric acid was used to prevent precipitation of lanthanide fluorides (24 g of

Received: March 16, 2011
Published: August 01, 2011

dx.doi.org/10.1021/ic2005453 | *Inorg. Chem.* 2011, 50, 8112–8120

citric acid and 4 mL of ethylene glycol per 1 g of product). During intensive stirring, an aqueous solution of ammonium fluoride was slowly dropped into the solution (with 25% excess due to the stoichiometric amounts of La^{3+} and Eu^{3+} ions). The solution was heated at 80 °C for 24 h in order to evaporate the water and to obtain a gel. Prepared in this manner, the precursor was calcined at 500−900 °C in an air atmosphere within 2 h.

Apparatus. Thermogravimetric (TG) analysis (TG) and differential thermal gravimetry (DTG) were performed using a Haas DSC XP-10i. X-ray diffraction patterns (XRD) were collected on a Bruker AXS D8 Advance diffractometer in Debye−Scherrer geometry, using Cu $K\alpha_1$ radiation (1.541874 Å) in 2θ ranges from 6° to 60°. The XRD results were compared with the Joint Committee on Powder Diffraction Standards (JCPDS) database. Average crystallite sizes were calculated from the Scherrer equation

$$D = \frac{0.9\lambda}{\cos\theta\sqrt{\beta^2 - \beta_0^2}} \quad (1)$$

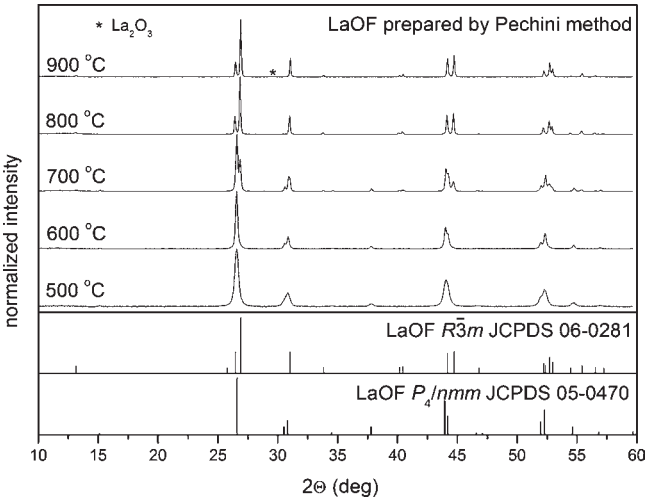

Figure 1. Influence of the annealing temperatures on the LaOF nanocrystals structure.

where D is the average grain size, the factor 0.9 is characteristic for spherical objects, λ is the X-ray wavelength, and θ and β are the diffraction angle and full-width at half-maximum of an observed peak. Cell parameters and phases quantities were calculated with the help of Rietveld analysis[24] using Maud 2.0 software.[25,26] The TEM images were measured in a JEM 1200 EXII, JEOL transmission electron microscope using an accelerating voltage of 80 kV.

Luminescence properties of the obtained samples were measured in a Hitachi F-7000 Fluorescence Spectrophotometer at room and liquid nitrogen temperatures (300 and 77 K) equipped with a 150 W xenon lamp. Excitation and emission spectra were corrected for the instrumental response and normalized to the intensity of the charge transfer band (excitation spectra) or the $^5D_0 \rightarrow {}^7F_2$ transition band (emission spectra).

Emission lifetimes were measured at 300 K using a monochromator (SpectraPro 275, Acton), a R955 photomultiplier (Hamamatsu), and a real-time digital oscilloscope (LeCroy, model Wave Runner 6100A). The Quanta-Ray GCR-11 Nd:YAG laser (Spectra Physics) laser operating at 266 nm was chosen as an excitation source.

RESULTS AND DISCUSSION

Structural Anaysis. The first structural investigations of the lanthanide oxyfluorides were performed by Zachariasen in 1951.[17] According to the published results, there are two LaOF phases. The crystal structure of LaOF has been found to be tetragonal P_4/nmm (no. 129) after annealing LaF_3 at 920 °C within 2−5.5 h and rhombohedral $R3\overline{m}$ (no. 166) after 10.5 h at the same temperature. According to Zachariasen, the tetragonal phase has a wide homogeneity range and an excess of fluorine ions, which stabilizes the structure. Nonstoichiometric tetragonal LaOF can be described by the formula LaO_nF_{3-2n}, where n ranges from 0.7 to 1.[17] Third, the cubic $F4\overline{m}$ (no. 216) structure of LaOF is also known.[14] The LaOF crystal structure can be delivered from the fluorite CaF_2 system with tetragonal and trigonal distortions of the CaF_2 cubic cell. In the tetragonal crystal structure, La^{3+} ions have C_{4v} site symmetry, whereas in the rhombohedral structure, La^{3+} occupy sites with C_{3v} symmetry.[19] Those differences have an influence on the Eu^{3+} luminescence in LaOF:Eu^{3+} material.

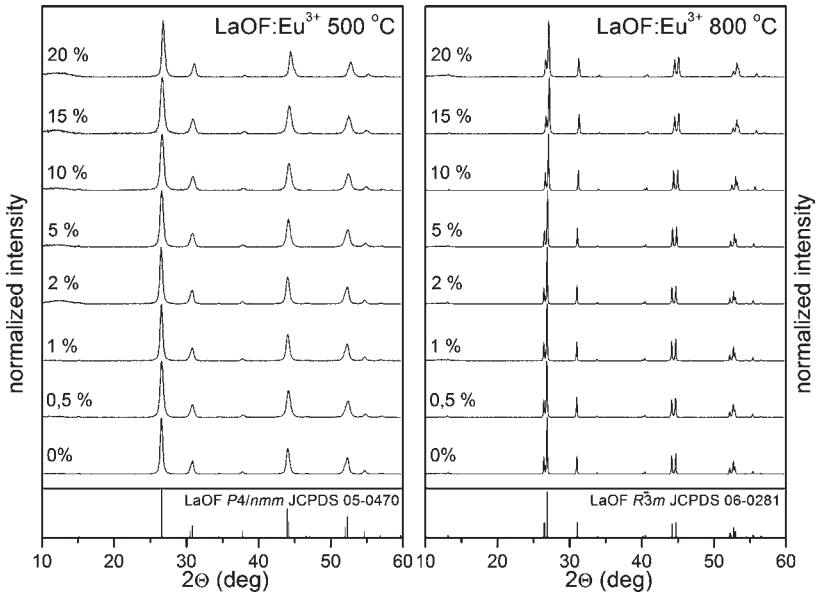

Figure 2. XRD patterns of tetragonal and rhombohedral LaOF:Eu^{3+} doped with 0.5−20% Eu^{3+}, prepared at 500 and 800 °C.

dx.doi.org/10.1021/ic2005453 |Inorg. Chem. 2011, 50, 8112–8120

Table 1. Rietveld Refinement Results of the Pure LaOF Samples Prepared in the 500−800 °C Range of Temperatures and Nanocrystal Sizes Calculated from the Scherrer Equation

	phase (%)			
temp. (°C)	tetragonal	rhombohedral	R_w (%)	grain size (nm)
500	99.88 ± 1.23	0.22 ± 1.11	3.43	20.2 ± 2.1
600	94.82 ± 0.37	5.18 ± 0.18	4.75	37.9 ± 5.0
700	80.03 ± 0.35	19.97 ± 0.12	3.81	47.0 ± 11.6
800	0.78 ± 0.23	99.22 ± 1.02	4.70	65.9 ± 10.5

Table 2. Results of the Rietveld Refinement and Nanocrystal Sizes of the LaOF:Eu^{3+} Samples Prepared at 500 and 800 °C

sample	a (Å)	c (Å)	V (Å^3)	R_w (%)	grain size (nm)
tetragonal LaOF prepared at 500 °C					
LaOF[a]	4.091	5.837	97.69		
LaOF	4.101(1)	5.851(8)	98.42	3.43	20.2 ± 2.1
LaOF:Eu^{3+} 0.5%	4.095(0)	5.844(8)	98.01	3.37	17.5 ± 3.2
LaOF:Eu^{3+} 1%	4.101(1)	5.852(9)	98.44	3.41	18.4 ± 2.9
LaOF:Eu^{3+} 2%	4.098(7)	5.848(0)	98.24	3.63	19.4 ± 1.8
LaOF:Eu^{3+} 5%	4.092(3)	5.836(1)	97.74	3.61	15.3 ± 1.7
LaOF:Eu^{3+} 10%	4.084(3)	5.827(5)	97.21	3.26	14.1 ± 2.9
LaOF:Eu^{3+} 15%	4.078(6)	5.818(0)	96.78	3.73	14.6 ± 2.5
LaOF:Eu^{3+} 20%	4.097(1)	5.847(2)	95.63	3.49	17.4 ± 5.3
rhombohedral LaOF prepared at 800 °C					
LaOF[a]	4.048	20.187	287.47		
LaOF	4.056(9)	20.227(1)	288.31	4.70	65.9 ± 10.5
LaOF:Eu^{3+} 0.5%	4.060(8)	20.236(0)	288.99	4.52	57.0 ± 6.4
LaOF:Eu^{3+} 1%	4.056(1)	20.223(2)	288.14	6.33	68.5 ± 3.8
LaOF:Eu^{3+} 2%	4.054(8)	20.218(3)	287.88	7.26	66.6 ± 11.2
LaOF:Eu^{3+} 5%	4.049(4)	20.192(3)	286.75	6.83	64.1 ± 4.8
LaOF:Eu^{3+} 10%	4.031(9)	20.106(7)	283.07	6.13	61.6 ± 3.2
LaOF:Eu^{3+} 15%	4.020(0)	20.045(0)	280.54	9.87	48.7 ± 5.7
LaOF:Eu^{3+} 20%	4.022(2)	20.052(1)	280.94	4.87	41.3 ± 4.2

[a] Crystal cell parameters from the JCPDS database.

The results of TG and DTG analyses indicated that up to 540 °C decomposition of the organic components of the precursor occurred, and therefore, annealing temperatures of prepared gel precursors have been chosen to be in the range 500−900 °C.

The XRD patterns of the prepared samples are presented in Figures 1 and 2. Table 1 contains results of the Rietveld refinement, concerning phase composition of the LaOF samples without any dopants.

Annealing of the gel precursor at 500 °C resulted in formation of the tetragonal phase. Increasing the reaction temperature induced changes in the phase's composition. Transformation from the tetragonal to the rhombohedral phase occurred, and at 800 °C, the latter phase was the dominant one. Annealing at intermediate temperatures led to a mixture of the above phases. With increasing temperature there was also an observed increase in the nanocrystal's size from around 20 to 65 nm. For further investigations, only the tetragonal and rhombohedral samples, prepared at 500 and 800 °C, respectively, were used. The calculations compiled in

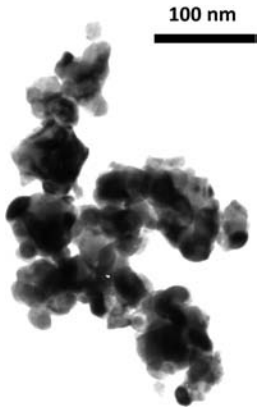

Figure 3. TEM image of the LaOF:Eu^{3+} 5% nanocrystals prepared at 600 °C.

Table 1 contain information about the crystals' sizes in the prepared oxyfluorides. Evidence for an annealing temperature effect on the crystal sizes was noted. Typically, higher temperatures caused growth of the nanocrystals and an increase in their sizes with temperature could be observed.

Figure 1 shows XRD patterns of pure LaOF, which are in good agreement with the JCPDS standards. The XRD patterns of the sample prepared at 900 °C show a small peak around 29.5 2θ (labeled with an asterisk (*)), probably derived from the La_2O_3 phase as a product of a thermal decomposition of LaOF.

Doping LaOF with Eu^{3+} ions had no noticeable effect on the structure except for the crystal cell dimensions, which decreased with increasing amounts of Eu^{3+}. The Eu^{3+} ion has a smaller ion radius than does La^{3+},[27] which is naturally responsible for those changes. Modifications of the crystal cell size had an influence on the peak positions of the XRD patterns shown in Figure 2. Table 2 presents the calculated crystal parameters for the tetragonal and rhombohedral samples. The refined crystal parameters are in accordance with the standards from the database. The unit cell size has a direct influence on the size of nanocrystals. A dependence of the nanocrystals' sizes on the volume of the crystal cell was observed.

The TEM image presented in Figure 3 shows a LaOF:Eu^{3+} 5% sample prepared at 600 °C. The morphology of crystals is in accordance with the data calculated from the broadening of the XRD reflections. A small distribution of the crystallite sizes can be observed, but most of the crystallites do not exceed 50 nm.

Luminescence Properties. In the spectroscopic studies of the LaOF:Eu^{3+} nanocrystals, the Eu^{3+} ion plays an important role as a luminescent probe. The properties of this ion can be used for investigating the relationship between luminescence and structure.[28] The emission spectra of the Eu^{3+}-doped LaOF is dominated by transitions from the $^5D_0$ level. Emission from higher levels can be also observed. It is possible because of the low phonon energy of the LaOF host. The probability for the multiphonon relaxation of the highest excited levels of Eu^{3+} ion is small, and therefore, quenching of the $^5D_2$ and $^5D_1$ levels is relatively small. The $^5D_0 \rightarrow {}^7F_2$ transition has the highest intensity in all samples.

Figure 4 presents changes in the excitation and emission spectra of the LaOF:Eu^{3+} 5% nanocrystals with increasing temperature of calcination. The broad charge transfer band (CT) dominated the excitation spectra. This characteristic band has also been observed in other compounds containing oxygen,

dx.doi.org/10.1021/ic2005453 |Inorg. Chem. 2011, 50, 8112–8120

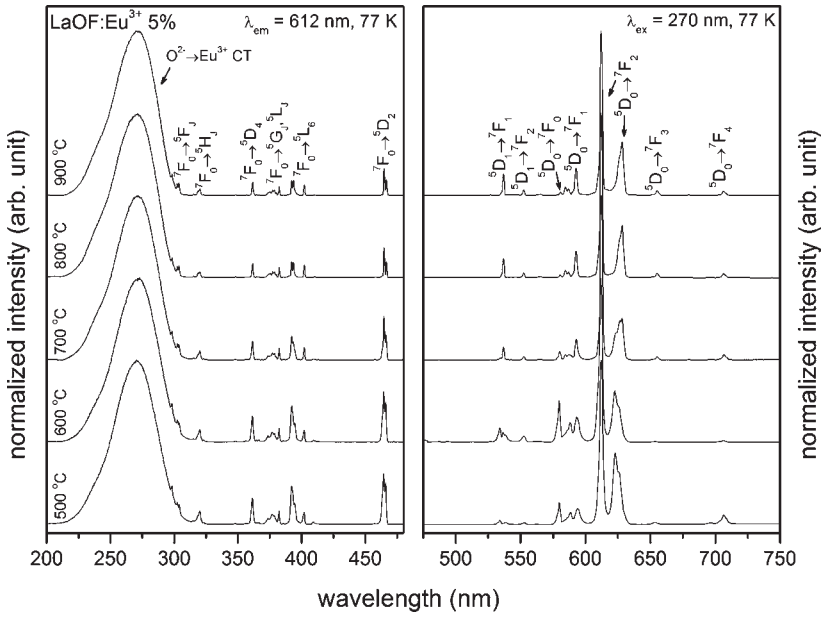

Figure 4. Temperature dependence on the excitation (left) and emission (right) spectra of LaOF:Eu^{3+} 5% nanocrystals, measured at 77 K.

and it is associated with $Eu^{3+}-O^{2-}$ interactions.[29] Also, narrow peaks, with relatively low intensity, can be observed. These bands are associated with the f−f transitions of the Eu^{3+} ion and are Laporte forbidden, which is responsible for their low intensities. All of the measured spectra were normalized to the CT intensity in the excitation spectra and to the $^5D_0 \rightarrow {}^7F_2$ transition in the luminescence spectra.

The CT energy could be estimated by using the following equation given by Jørgensen[30]

$$E_{CT} = [\chi(L) - \chi(M)](3 \times 10^4) \quad (2)$$

where E_{CT} denotes the position of the CT band (in cm^{-1}) and χ(L) and χ(M) are the optical electronegativity of the anion and the central metal cation. For χ(O) = 3.2 and χ(Eu) = 1.75, the calculated CT position should be 42 000 cm^{-1} (around 238 nm). The measured positions of the CT band in the obtained sample bands were around 270 nm. The red shift of the CT band results from a difference between bulk materials, for which eq 2 was evaluated, and nanosized phosphors. In the LaOF:Eu^{3+} nanocrystals, the energy for ionization of the O^{2-} ion was lower due to the higher energy of the transferred electron.[31]

Figure 4 shows also the emission from the LaOF:Eu^{3+} 5% nanocrystals obtained at different temperatures. In contrast to the excitation spectra, changes of the positions and intensities of the emission peaks are more prominent. The electronic transitions $^5D_0 \rightarrow {}^7F_J$ (J = 0−4) dominate the spectra, but also transitions from the higher excited states $^5D_1$ and $^5D_2$ could be observed. The electric dipole $^5D_0 \rightarrow {}^7F_2$ transition had the highest emission intensity, and the splitting of this level was larger in the rhombohedral than in the tetragonal host. The intensity of the magnetic dipole transition $^5D_0 \rightarrow {}^7F_1$ was low in all of the measured spectra and generally was low in all REOF hosts.[32] The $^5D_0 \rightarrow {}^7F_0$ transition intensity decreases noticeably with increasing annealing temperature, which distinguishes the tetragonal phase from the rhombohedral phase. This transition is forbidden by the selection rules of f−f transitions, but it could be observed when the Eu^{3+} ions occupy a site with C_s, C_n, or C_{nv} symmetry through $J-J'$ mixing effects.[33,34] The lower intensities in the rhombohedral host have been explained by the proximity of the T_d pseudosymmetry for the Eu^{3+} site in which the $^5D_0 \rightarrow {}^7F_0$ transition is forbidden.[19]

Excitation spectra of both types of LaOF:Eu^{3+} structures are presented in Figures 5 and 6. The most visible changes appear in the Eu^{3+} transitions region, where excitation from the $^7F_0$ to higher excited levels occurs. The successive increase in the intensity of these peaks with increasing Eu^{3+} concentration can be noted. Also, in the CT band, some changes can be observed. First, there is a significant broadening of the CT band when the Eu^{3+} concentration increases. It is caused by the growing number of slightly distorted Eu^{3+} sites (e.g., on the nanocrystals surface) and therefore small $Eu^{3+}-O^{2-}$ distance changes, which have a direct influence on the CT band shape. Also, there was a small red shift, which was particularly apparent in the rhombohedral structure. This second phenomenon is due to the changes in the size of the nanocrystals, which are larger in rhombohedral LaOF:Eu^{3+}.

Emission spectra of the samples prepared at 500 and 800 °C are also presented at Figures 5 and 6. Most of the changes occur in parts of the spectra where transitions from higher levels ^5D_J (J = 1−3) can be observed. These transitions are sensitive to the cross-relaxation process caused by high Eu^{3+} concentrations. The higher manifolds can also take part in the energy transfer between Eu^{3+} ions, which is discussed further below. With increasing concentration of Eu^{3+} ions in the LaOF lattice, the emission associated with the $^5D_1 \rightarrow {}^7F_1$ transition decreases remarkably and disappears when the dopant concentration is higher than 10% in tetragonal and 20% in rhombohedral LaOF.

From the comparison between the $^5D_0 \rightarrow {}^7F_2$ integrated luminescence intensity of the LaOF:Eu^{3+} samples (Figure 7), the best dopant concentration could be determined. The highest intensity was measured for the 5%-doped tetragonal and the 10%-doped rhombohedral LaOF host.

Luminescence Decays. Luminescence decays of tetragonal and rhombohedral LaOF:Eu^{3+} were measured at room temperature for different concentrations of the Eu^{3+} ion at 612 nm

dx.doi.org/10.1021/ic2005453 |Inorg. Chem. 2011, 50, 8112–8120

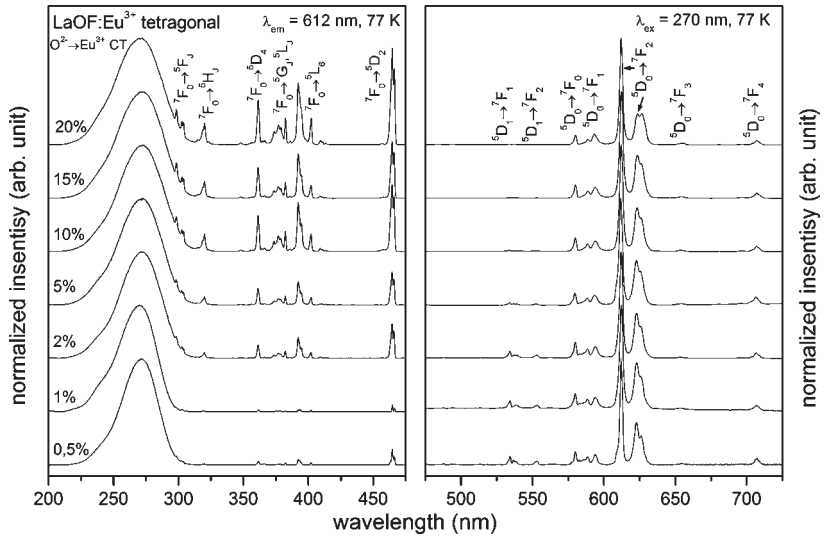

Figure 5. Effect of Eu^{3+} concentration on the excitation (left) and emission (right) spectra of tetragonal LaOF:Eu^{3+} nanocrystals measured at 77 K.

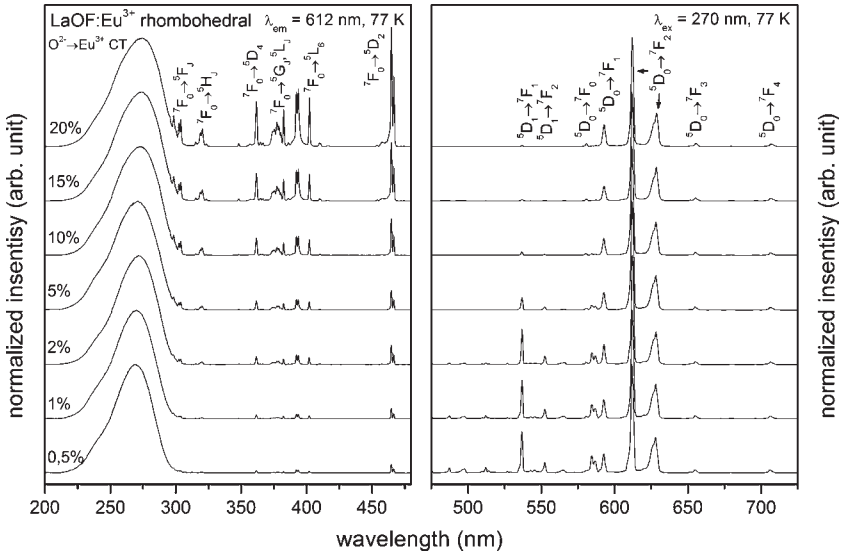

Figure 6. Effect of the Eu^{3+} concentration on the excitation (left) and emission (right) spectra of rhombohedral LaOF:Eu^{3+} nanocrystals measured at 77 K.

corresponding to the $^5D_0 \rightarrow {}^7F_2$ transition band. The emission decay profiles are shown in Figures 8 and 9. In both hosts a conspicuous increase in the luminescence intensity with time could be observed. Similar results have been reported earlier,[35−37] but this phenomenon is still not fully explained due to the complex behavior and involved mechanisms. The appearance of the rise time indicates the presence of a slow relaxation processes feeding the emitting level.

Several relaxation models can be applied to explain processes taking place after excitation of the sample. In the investigation by Tallant et al.,[35] Y_2O_3 host with low Eu^{3+} concentration (<1%), population of the $^5D_3$ manifold occurred by fast relaxation from the CT, 5d, and upper 4f manifolds (Figure 10, mechanism I). Then slower sequential relaxation to the emitting level takes place, increasing the luminescence. In principle, this process should be independent of the Eu^{3+} concentration. The observed LaOF:Eu^{3+} decay times significantly shortened with increasing concentration of Eu^{3+}, which suggests that the rise time must be associated with other, cooperative processes. In previous studies, Tallant[35] and Zych[36] proposed a different mechanism based on energy transfer from one Eu^{3+} ion in an excited ^5D_J ($J > 0$) manifold to another Eu^{3+} in the ^7F_J ground state. As a result of this interaction, donor ion undergoes to the $^5D_0$ excited state and $^5D_0 \rightarrow {}^7F_2$ emission is observed, while an acceptor is excited to the F_J ($J > 0$) level, which nonradiatively relaxes to the ground state (Figure 10, mechanism II). This process affected the relaxation dynamics but did not affect the quantum yield.[35,37]

The scheme in Figure 10 illustrates a cross relaxation between two Eu^{3+} (donor and acceptor) ions according to the suggested mechanism II. The extent of the ^7F manifold is about 5000 cm^{-1}, which is large enough for accommodation of the energy associated with relaxation also from the $^5D_2$ or $^5D_3$ levels. However, in the higher Eu^{3+}-doped host also interaction between two donors is possible. In this situation, one of the excited Eu^{3+} ions transfers its entire energy to another excited Eu^{3+} ion in its $^5D_0$ state, doubling its energy (mechanism III). The activator in the

dx.doi.org/10.1021/ic2005453 |Inorg. Chem. 2011, 50, 8112–8120

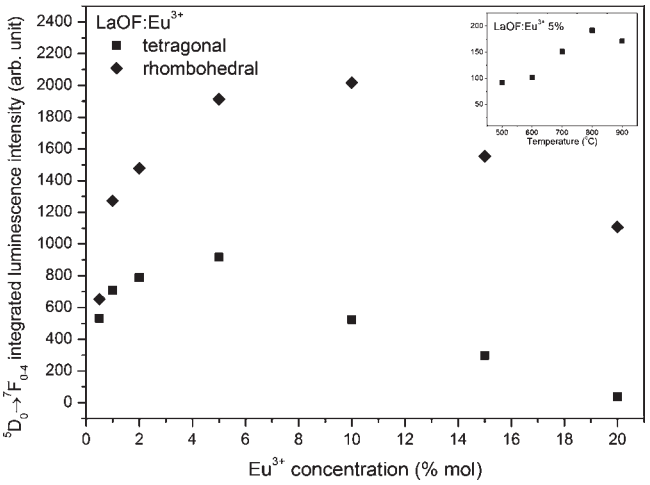

Figure 7. Comparison of the integrated luminescence intensity from the $^5D_0$ level of the prepared LaOF:Eu^{3+} samples with changing concentration of the Eu^{3+} ion; excitation wavelength λ_{ex} = 270 nm.

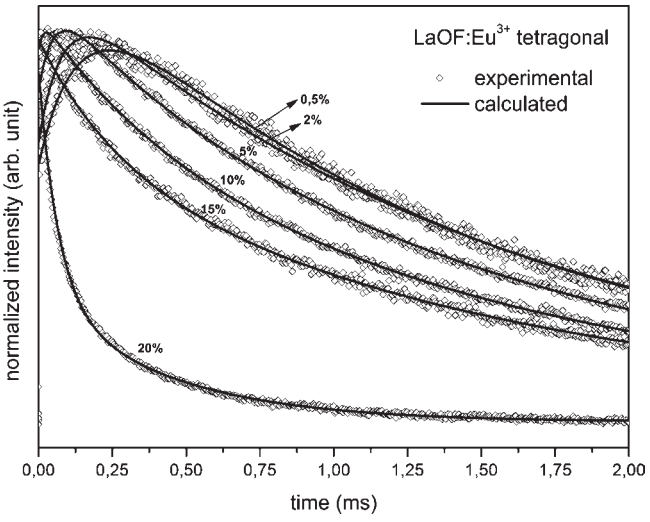

Figure 8. Decay time curves of tetragonal LaOF:Eu^{3+} measured at 300 K, λ_{ex} = 266 nm.

upper excited state (upper f levels) relaxes to the ^5D_J manifold by a nonradiative path. This process decreases the quantum efficiency of the phosphor, since instead of the emission of two photons after energy transfer only one can be emitted.

Measured decay profiles were fitted using the following equation

$$I = [I_0 + I_1(1 - e^{-t/\tau_r})]e^{-t/\tau_d} \quad (3)$$

where I_0 is an initial luminescence intensity at time $t = 0$, I_1 is an intensity added by energy transfer, and τ_r and τ_d are rise and decay times. This equation fit well to the decay profiles of the samples with lower Eu^{3+} concentrations. For the 5%-doped tetragonal, 5% and 10% rhombohedral LaOF, eq 3 has been modified because of an additional component appearing in the decays

$$I = [I_0 + I_1(1 - e^{-t/\tau_r})]e^{-t/\tau_{d1}} + [I'_0 + I'_1(1 - e^{-t/\tau_r})]e^{-t/\tau_{d2}} \quad (4)$$

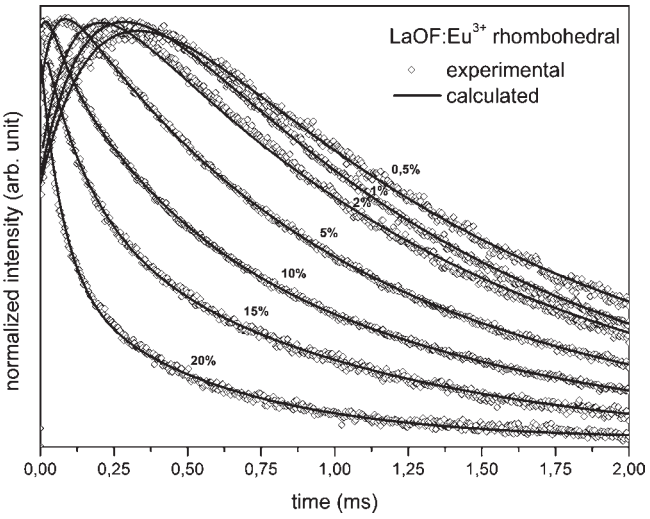

Figure 9. Decay time curves of rhombohedral LaOF:Eu^{3+} measured at 300 K, λ_{ex} = 266 nm.

where I'_0 and I'_1 are intensities connected with a second component and τ_{d1} and τ_{d2} are decay times of the two different components. Moreover, in the samples with an Eu^{3+} concentration above 10%, the rise time disappeared and in order to fit these decay curves a simple biexponential function was applied

$$I = I_0 e^{-t/\tau_{d1}} + I'_0 e^{-t/\tau_{d2}} \quad (5)$$

The results of the fitting are presented in Table 3.

The reported results indicate that the rise time depends on the Eu^{3+} concentration, which excludes mechanism I as an explanation of the growing-in of the luminescence with time for the samples doped higher than 0.5% of Eu^{3+}. The observed quenching of the emission from the $^5D_1$ level with increasing concentration of Eu^{3+} ions evidences the energy transfer by proposed mechanism II. Additional measurements of the emission spectra (Figure 11) with excitation at 580 nm ($^5D_0$ level) confirmed that mechanism III is also involved in the energy transfer processes, however only in the rhombohedral LaOF:Eu^{3+}. The radiation used, with wavelength $\lambda \approx 580$ nm, should be absorbed by a sample generating Eu^{3+} in the $^5D_0$ excited state. According to mechanism III, Eu^{3+} ions interact and therefore energy transfer between them occurs. After this process one of the ions (Eu1) remains in the ground state while the second one (Eu2) transfers to the excited state of energy higher than $^5D_0$. Then nonradiative relaxations of higher excited Eu^{3+} provide to ions in one of the ^5D_J ($J = 0-3$) excited states from which emission could be observed. Upconversion emission from higher ^5D_J levels was observed only for rhombohedral samples with Eu^{3+} concentration from 1% to 10%, which confirms the occurrence of interactions consistent with mechanism III. It is clearly evidenced that only interactions in accordance with mechanism II could be responsible for the observed decay profiles in the tetragonal LaOF:Eu^{3+}. In the rhombohedral host, both mechanisms II and III are probably responsible for the build-up rates. For the disparity between discussed hosts, only differences in crystal sizes could be responsible (distances between Eu^{3+} ions in both hosts are comparable).

Decreasing rise times suggest that the time for energy migration between Eu^{3+} ions is shortening with increasing dopant concentration and finally disappears when the Eu^{3+} ions in the

dx.doi.org/10.1021/ic2005453 |Inorg. Chem. 2011, 50, 8112–8120

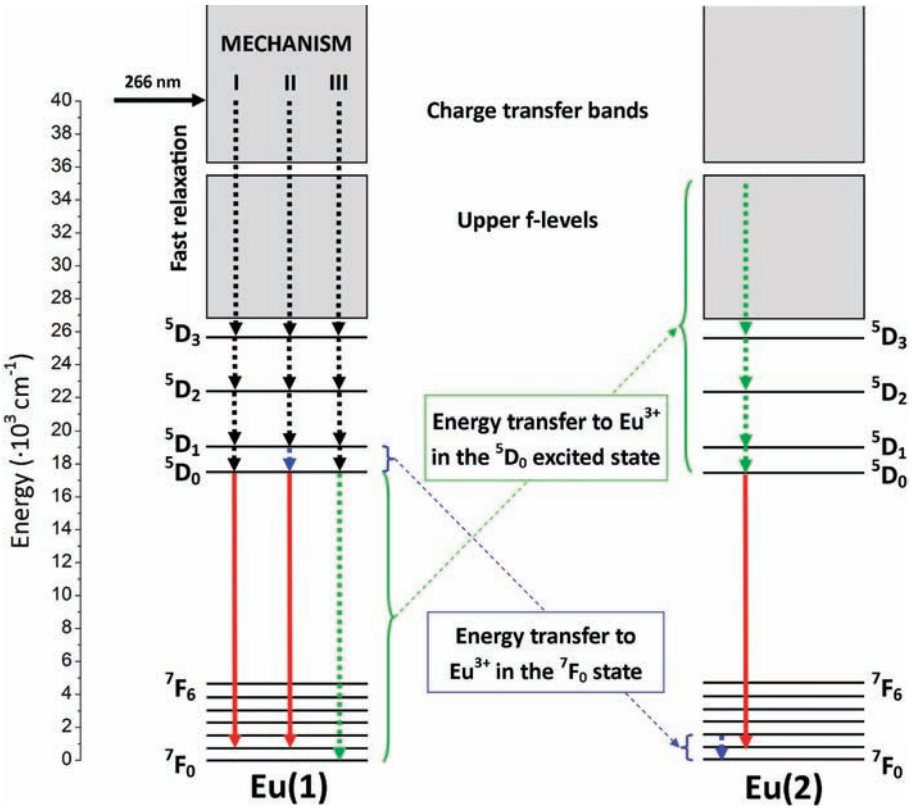

Figure 10. Scheme of the possible relaxation and energy transfer models in the Eu^{3+}-doped host.

Table 3. Results of the Calculations Judd−Ofelt Intensity Parameters (Ω_2, Ω_4) Determined from Luminescence Spectra Decay Rates and Quantum Efficiencies of Luminescence[a]

temp. (°C)	Eu (%)	τ_r (ms)*	τ_{d1} (ms)	τ_{d2} (ms)	A_{rad} (s^{-1})	A_{nrad} (s^{-1})	A_{tot} (s^{-1})	Ω_2 (10^{-20} cm^2)	Ω_4 (10^{-20} cm^2)	η (%)
500	0.5	0.146(8)	1.394(4)		681	39	719	58.2	13.8	95
	1	0.120(0)	1.473(4)		663	17	680	56.3	13.9	97
	2	0.084(0)	1.558(6)		637	4	641	53.8	13.1	99
	5	0.025(9)	1.483(2)		675	1	676	57.5	13.9	100
	10	0.014(8)	1.600(4)	0.416(5)	663	8	671	56.7	13.3	99
	15		1.541(2)	0.261(0)	679	11	690	57.8	14.3	98
	20		0.427(5)	0.066(3)	673	2184	2857	57.5	13.8	24
800	0.5	0.259(2)	1.268(6)		679	108	787	61.5	8.9	86
	1	0.210(7)	1.220(6)		745	75	820	67.9	10.3	91
	2	0.118(6)	1.293(2)		671	104	775	61.1	8.5	87
	5	0.048(0)	1.580(3)	0.714(0)	747	5	752	68.4	10.0	99
	10	0.035(1)	1.350(2)	0.380(6)	740	94	833	67.6	9.7	89
	15		1.385(3)	0.372(3)	836	354	1190	77.1	11.1	70
	20		0.993(4)	0.157(7)	861	1222	2083	79.0	12.3	41

[a] Maximum calculations' errors: τ_r 0.00168 ms, τ_{d1} 0.00227 ms, τ_{d2} 0.00108 ms; η 8,9%.

LaOF host was higher than 10% (in fact, probably it is very fast and could not be observed). High Eu^{3+} concentrations and decreasing nanocrystal sizes are the reasons why the second component of the decay appears. The relatively high proportion of surface to volume for the nanocrystals causes, statistically, many of the Eu^{3+} ions to occupy sites on or near the surface. To determine which of the remaining mechanisms is responsible for the build-up times, it is necessary to calculate the quantum efficiency, which was done using Judd−Ofelt calculations.

Judd−Ofelt Parameters. The nature of the luminescence behavior of Eu^{3+} in the LaOF host can be investigated by an analysis of the intensity parameters Ω_2, Ω_4, and Ω_6. To our knowledge, there is no report on the calculation of the Judd−Ofelt parameters for the LaOF:Eu^{3+} compound. According to the Judd−Ofelt theory,[38,39] intensity parameters contain contributions from the forced electric dipole and dynamic coupling mechanisms. These parameters can be calculated from emission spectra, following the method described previously by

dx.doi.org/10.1021/ic2005453 |*Inorg. Chem.* 2011, 50, 8112–8120

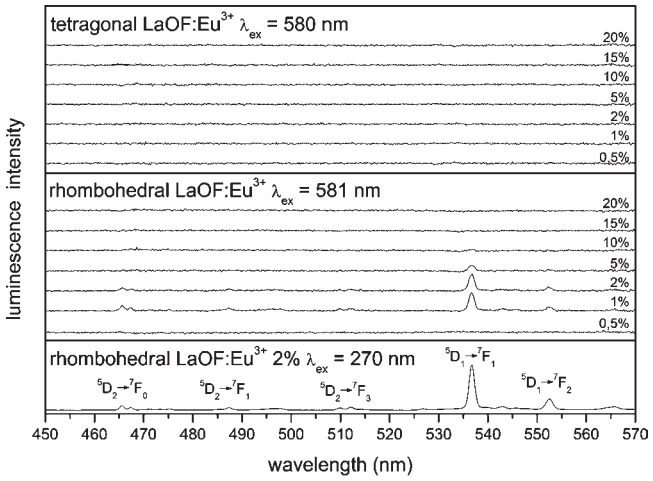

Figure 11. Luminescence of tetragonal and rhombohedral LaOF:Eu^{3+} after excitation at the $^5D_0$ level, and reference spectra of the rhombohedral LaOF:Eu^{3+} 2% sample using a 270 nm excitation source.

Kodaira et al.[40] and subsequently used by others.[41] In this method, the integrated coefficients of the spontaneous emission of the transition between two manifolds $^5D_0$ and ^7F_J (J = 2, 4, 6) can be obtained experimentally from the relationship

$$A_{0-\lambda} = A_{0-J} = A_{0-1}\frac{I_{0-J}h\nu_{0-1}}{I_{0-1}h\nu_{0-J}} \quad (6)$$

where I_{0-J} and I_{0-1} are integral intensities for $^5D_0 \rightarrow {}^7F_J$ and $^5D_0 \rightarrow {}^7F_1$ transitions and $h\nu_{0-J}$ and $h\nu_{0-1}$ are their energies, respectively. Due to the magnetic character of the $^5D_0 \rightarrow {}^7F_1$ transition and its weak dependence on crystal field effects, the value of the A_{0-1} coefficient was estimated to be about 50 s^{-1}.[42] The Ω_6 intensity parameter was not calculated because the $^5D_0 \rightarrow {}^7F_6$ transition could not be observed. In the Judd−Ofelt theory, the Einstein coefficient $A_{0-\lambda}$ of the spontaneous emission is expressed as

$$A_{0-\lambda} = \frac{64\pi^4\nu^3e^2}{3hc^3}\frac{1}{4\pi\varepsilon_0}\chi\sum_{\lambda=2,4}\Omega_\lambda\langle {}^5D_0\left\|U^{(\lambda)}\right\|{}^7D_J\rangle^2 \quad (7)$$

where $\langle {}^5D_0||U^{(\lambda)}||{}^7F_J\rangle^2$ are the square reduced matrix elements whose values are independent of the chemical environment of the Eu^{3+} ion. Their values were known and are $\langle {}^5D_0||U^{(4)}||{}^7F_4\rangle^2$ = 0.0032 and $\langle {}^5D_0||U^{(2)}||{}^7F_2\rangle^2$ = 0.0023.[43] $\chi = n_0(n_0^2 + 2)/9$ is the Lorentz local field correction and n_0 is a refraction index (the value used for the calculation was taken from ref 44 as equal to 1.8). From the calculated radiative rates for each transition, it is possible to evaluate the radiative decay rate (A_{rad})

$$A_{rad} = \sum_J A_{0-J} \quad (8)$$

Measuring luminescence decays, the nonradiative (A_{nrad}) and total (A_{tot}) coefficients can be calculated from the following equation

$$A_{tot} = \frac{1}{\tau} = A_{rad} + A_{nrad} \quad (9)$$

The emission quantum efficiency of the emitting $^5D_0$ level is given by

$$\eta = \frac{A_{rad}}{A_{rad} + A_{nrad}} \quad (10)$$

Since the luminescence decay kinetics is nonexponential, average lifetimes were used for calculations by applying the equation[45,46]

$$\tau = \frac{I_0\tau_{d1}^2 + I_0'\tau_{d2}^2}{I_0\tau_{d1} + I_0'\tau_{d2}} \quad (11)$$

Results of the calculations are summarized in Table 3. The Judd−Ofelt parameters are relatively large, but it has been observed that nanocrystalline samples usually have higher values compared to their bulk counterparts.[3,47] This behavior could be explained by the fact that for the nanocrystalline samples a higher fraction of the Eu^{3+} ions is on the surface of the nanocrystals than in the bulk materials. Hence, the average crystal field effect on the Eu^{3+} ions in the nanocrystals is different compared to the bulk samples. The hypersensitive $^5D_0 \rightarrow {}^7F_2$ transition is mainly responsible for the Ω_2 value, and it depends on short distance effects. In both hosts this parameter is large, which is typical for strongly polarizable environments of the Eu^{3+} ions. The value of the parameter Ω_2 is larger for a rhombohedral host where additional increases are seen with growing Eu^{3+} concentration.

Analysis of the changes of parameter Ω_2 can be informative about distortions around occupied Eu^{3+} ion sites. The relative intensity of the electric dipole $^5D_0 \rightarrow {}^7F_2$ transition depends on the local symmetry of the Eu^{3+} ions. The intensity of this transition increases with decreasing local symmetry of the Eu^{3+} ion, which directly influences the value of the Ω_2 parameter. The environment of the Eu^{3+} sites is different in the hosts, under discussion, which was mentioned previously. The value of the Ω_2 parameter is higher for the rhombohedral LaOF, where the Eu^{3+} ions occupy sites with lower symmetry (C_{3v}) than in the tetragonal lattice (C_{4v}). Also, changes with increasing Eu^{3+} concentration were observed. This behavior is associated with the decreasing crystal cell volume as well as with the decreasing nanocrystals sizes, and therefore, higher amounts of the Eu^{3+} ions on the surface of the nanocrystals in the asymmetric environment occur. Higher Ω_2 for the rhombohedral LaOF also suggests greater electrostatic character of the metal−donor interactions in this lattice.

In the case of Ω_4 the situation is reversed; larger values were obtained for the tetragonal host. The parameter Ω_4 is not directly related to the symmetry of the Eu^{3+} ion but to the electron density on the surrounding ligands, and its value decreases when the electron density on the ligands increases. Larger values in the tetragonal LaOF also support the deduction about more covalency of the Eu^{3+}−O^{2-} bonds in this lattice.

The prepared LaOF:Eu^{3+} shows a high quantum yield of luminescence except those where the activator concentration is 20%. Energy transfer processes observed in the decay curves could enhance the quantum efficiency of the prepared nanophosphors.

CONCLUSIONS

Nanocrystalline LaOF:Eu^{3+} can be successfully synthesized by the sol−gel Pechini method. This convenient method gave materials with intense luminescence and the expected (desired) morphology. The best conditions for annealing of the precursors were found to be 500 °C for tetragonal and 800 °C for rhombohedral nanocrystals. From an analysis of the luminescent properties, the best dopant concentrations were established to be 5% for tetragonal and 10% for rhombohedral LaOF. The calculated values of quantum efficiencies were close to 100% in almost all samples. For the first time the processes of energy

dx.doi.org/10.1021/ic2005453 |Inorg. Chem. 2011, 50, 8112–8120

transfer between Eu^{3+} ions in LaOF have been analyzed, appearing in rise times of the luminescence. In order to investigate the nature of the intense luminescence of Eu^{3+} in both LaOF hosts, the Judd−Ofelt intensity parameters were calculated from the experimental data. From the small quenching of the LaOF matrix, the profiles of luminescence decays, and their dependence on the concentration of the Eu^{3+} ions as well as the large quantum yields of luminescence it can be concluded that for the build-up time of the luminescence mechanism II is mainly responsible. However, in the rhombohedral samples, a noticeable effect of mechanism III on the luminescent properties of the investigated nanophosphors could be also observed.

AUTHOR INFORMATION

Corresponding Author

*Phone: +48 61 8291345. E-mail: blis@amu.edu.pl.

ACKNOWLEDGMENT

T.G. gratefully acknowledges the financial support in the form of the VENTURES project operated by the Foundation for Polish Science and financed by the EU European Regional Development Fund, Ventures/2009-4/2. The authors would like to thank Dr. T. Pedzinski (Adam Mickiewicz University) for his help in measurements of the luminescence decay times.

REFERENCES

(1) Lammers, M. J. J.; Blasse, G. *Phys. Status Solidi B* **1985**, *127*, 663–671.
(2) Hölsä, J.; Kestilä, E. *J. Alloys Compd.* **1995**, *225*, 89–94.
(3) Boyer, J. C.; Vetrone, F.; Capobianco, J. A.; Speghini, A.; Bettinelli, M. *J. Phys. Chem. B* **2004**, *108*, 20137–20143.
(4) Karbowiak, M.; Mech, A.; Kempiński, L.; Mielcarek, W.; Hubert, S. *J. Alloys Compd.* **2005**, *400*, 67–75.
(5) Bai, X.; Song, H.; Pan, G.; Lei, Y.; Wang, T.; Ren, X.; Lu, S.; Dong, B.; Dai, Q.; Fan, L. *J. Phys. Chem. C* **2007**, *111*, 13611–13617.
(6) Evanics, F.; Diamente, P. R.; Veggel, F. C.; van, J. M.; Stanisz, G. J.; Prosser, R. S. *Chem. Mater.* **2006**, *18*, 2499–2505.
(7) Psuja, P.; Hreniak, D.; Strek, W. *J. Nanomater.* **2007**, *2007*, 1–8.
(8) Peng, M.; Pei, Z.; Hong, G.; Su, Q. *Chem. Phys. Lett.* **2003**, *371*, 1–6.
(9) Mi, C.; Zhang, J.; Gao, H.; Wu, X.; Wang, M.; Wu, Y.; Di, Y.; Xu, Z.; Mao, C.; Xu, S. *Nanoscale* **2010**, *2*, 1141–1148.
(10) Mahakhode, J. G.; Dhoble, S. J.; Joshi, C. P.; Moharil, S. V. *J. Alloys Compd.* **2007**, *438*, 293–297.
(11) Zhang, X.; Gao, D.; Li, L. *J. Appl. Phys.* **2010**, *107*, 123528.
(12) He, E.; Zheng, H.; Zhang, Z.; Zhang, X.; Xu, L.; Fu, Z.; Lei, Y. *J. Nanosci. Nanotechnol.* **2010**, *10*, 1908–1912.
(13) Fujihara, S.; Kato, T.; Kimura, T. *J. Mater. Sci. Lett.* **2001**, *20*, 687–689.
(14) Deb, K. K.; Buser, R. G.; Morrison, C. A.; Leavitt, R. P. *J. Opt. Soc. Am.* **1981**, *71*, 1463.
(15) Hölsä, J. *Spectrochim. Acta, Part A* **1993**, *49*, 465–470.
(16) Gao, D.; Zheng, H.; Zhang, X.; Fu, Z.; Zhang, Z.; Tian, Y.; Cui, M. *Appl. Phys. Lett.* **2011**, *98*, 011907.
(17) Zachariasen, W. H. *Acta Crystallogr.* **1951**, *4*, 231–236.
(18) Antic-Fidancev, E.; Hölsä, J.; Krupa, J.-C.; Lastusaari, M. *J. Alloys Compd.* **2004**, *380*, 303–309.
(19) Hölsä, J. *Acta Chem. Scand.* **1991**, *45*, 583–587.
(20) Lee, J.; Zhang, Q.; Saito, F. *J. Alloys Compd.* **2003**, *348*, 214–219.
(21) Du, Y.-P.; Zhang, Y.-W.; Sun, L.-D.; Yan, C.-H. *J. Phys. Chem. C* **2008**, *112*, 405–415.
(22) Du, Y.-P.; Zhang, Y.-W.; Yan, Z.-G.; Sun, L.-D.; Yan, C.-H. *J. Am. Chem. Soc.* **2009**, *131*, 16364–5.
(23) Pechini, M. U.S. Patent No. 3330697, 1967.
(24) Rietveld, H. M. *J. Appl. Crystallogr.* **1969**, *2*, 65–71.
(25) Lutterotti, L.; Bortolotti, M. *Compcomm. Newslett.* **2003**, *1*, 43–50.
(26) Lutterotti, L. *Nucl. Instrum. Methods B* **2010**, *268*, 334–340.
(27) Shannon, R. *Acta Crystallogr., Sect. A* **1976**, *32*, 751.
(28) Binnemans, K.; Görller-Walrand, C. *J. Rare Earths* **1996**, *14*, 173–180.
(29) Dorenbos, P. *J. Phys.: Condes. Matter* **2003**, *15*, 8417–8434.
(30) Klixbüll Jørgensen, C. *Electron Transfer Spectra*; John Wiley & Sons, Inc.: New York, 1970; pp 101−158.
(31) Shang, C.; Shang, X.; Qu, Y.; Li, M. *Chem. Phys. Lett.* **2011**, *501*, 480–484.
(32) Hölsä, J.; Kestilä, E. *J. Alloys Compd.* **1995**, *225*, 89–94.
(33) Fong, F.; Vredevoe, L.; De Wames, R. *Phys. Rev.* **1968**, *170*, 412–417.
(34) Malta, O. *J. Lumin.* **1982**, *26*, 337–343.
(35) Tallant, D. R.; Seager, C. H.; Simpson, R. L. *J. Appl. Phys.* **2002**, *91*, 4053.
(36) Zych, E.; Hreniak, D.; Strek, W. *J. Phys. Chem. B* **2002**, *106*, 3805–3812.
(37) Joly, A.; Chen, W.; Zhang, J.; Wang, S. *J. Lumin.* **2007**, *126*, 491–496.
(38) Judd, B. *Phys. Rev.* **1962**, *127*, 750–761.
(39) Ofelt, G. S. *J. Chem. Phys.* **1962**, *37*, 511.
(40) Kodaira, C. *J. Lumin.* **2003**, *101*, 11–21.
(41) Wiglusz, R. J.; Pazik, R.; Lukowiak, A.; Strek, W. *Inorg. Chem.* **2011**, 300–301.
(42) Sá, G.; de; Donegá, C. M.; Malta, O. L.; Simas, A. M.; Longo, R. L.; Santa-Cruz, P. A.; Silva, E. F. da *Coord. Chem. Rev.* **2000**, *196*, 165–195.
(43) Carnall, W. T.; Crosswhite, H.; Crosswhite, H. M. *Energy level structure and transition probabilities in the spectra of the trivalent lanthanides in LaF3*; Argonne National Laboratory Report, 1978; Vol. *1*.
(44) Podberezskaya, N. V.; Batsanova, L. R.; Egorova, L. S. *J. Struct. Chem.* **1966**, *6*, 815–18.
(45) Lakowicz, J. R. *Principles of Fluorescence Spectroscopy*, 3rd ed.; Springer: Singapore, 2006; p 99.
(46) Kumar, K. U.; Prathyusha, V. A; Babu, P.; Jayasankar, C. K.; Joshi, A S.; Speghini, A.; Bettinelli, M. *Spectrochim. Acta, A* **2007**, *67*, 702–8.
(47) Liu, C.; Liu, J.; Dou, K. *J. Phys. Chem. B* **2006**, *110*, 20277–81.